Chemical and structural changes in Ln2NiO4+δ (Ln=La, Pr or Nd) lanthanide nickelates as a function of oxygen partial pressure at high temperature

Aurélien Flura, Sophie Dru, Clément Nicollet, Vaibhav Vibhu, Sébastien Fourcade, Eric Lebraud, Aline Rougier, Jean-Marc. Bassat, Jean-Claude Grenier

▶ **To cite this version:**

Aurélien Flura, Sophie Dru, Clément Nicollet, Vaibhav Vibhu, Sébastien Fourcade, et al.. Chemical and structural changes in Ln2NiO4+δ (Ln=La, Pr or Nd) lanthanide nickelates as a function of oxygen partial pressure at high temperature. Journal of Solid State Chemistry, 2015, 228, pp.189-198. 10.1016/j.jssc.2015.04.029 . hal-01158077

HAL Id: hal-01158077
https://hal.science/hal-01158077

Submitted on 2 Nov 2023

HAL is a multi-disciplinary open access archive for the deposit and dissemination of scientific research documents, whether they are published or not. The documents may come from teaching and research institutions in France or abroad, or from public or private research centers.

L'archive ouverte pluridisciplinaire **HAL**, est destinée au dépôt et à la diffusion de documents scientifiques de niveau recherche, publiés ou non, émanant des établissements d'enseignement et de recherche français ou étrangers, des laboratoires publics ou privés.

Chemical and structural changes in $Ln_2NiO_{4+\delta}$ (Ln=La, Pr or Nd) lanthanide nickelates as a function of oxygen partial pressure at high temperature

Flura Aurélien, Dru Sophie, Nicollet Clément, Vibhu Vaibhav, Fourcade Sébastien, Lebraud Éric, Rougier Aline, Bassat Jean-Marc, Grenier Jean-Claude

Affiliation : *CNRS, University of Bordeaux, ICMCB-CNRS, 87 Av. du Dr A. Schweitzer, Pessac-Cedex F-33600, France*

Abstract

The chemical stability of lanthanide nickelates $Ln_2NiO_{4+\delta}$ (Ln=La, Pr or Nd) has been studied in the temperature range 25–1300 °C, either in air or at low pO_2 (down to 10^{-4} atm). Thermal gravimetry analysis (TGA) measurements coupled with X-ray diffraction (XRD) characterization have shown that all compounds retain their K_2NiF_4-type structure in these conditions, while remaining over-stoichiometric in oxygen up to 1000 °C. Only $Nd_2NiO_{4+\delta}$ starts to decompose into Nd_2O_3 and NiO above 1000 °C, at $pO_2=10^{-4}$ atm. In addition, a careful analysis of the lanthanide nickelates structural features has been performed by *in situ* XRD, as a function of temperature and pO_2. For all compounds, a structural transition has been always observed in the temperature range 200–400 °C, in air or at $pO_2=10^{-4}$ atm. In addition, their cell volume did not vary upon the variation of the oxygen partial pressure. Therefore, these materials do not exhibit a chemical expansion in these conditions, which is beneficial for a fuel cell application as cathode layers. Additional dilatometry measurements have revealed that a temperature as high as 950 °C for $Pr_2NiO_{4+\delta}$ or 1100 °C for $La_2NiO_{4+\delta}$ and $Nd_2NiO_{4+\delta}$ has to be reached in order to begin the sintering of the material particles, which is of primary importance to obtain an efficient electronic/ionic conduction in the corresponding designed cathode layers. Besides, excellent matching was found between the thermal expansion coefficients of lanthanide nickelates and SOFC electrolytes such as 8wt% yttria stabilized zirconia (8YSZ) or $Ce_{0.8}Gd_{0.2}O_{2-\delta}$ (GDC), at least from 400 °C up to 1400 °C in air or up to 1200 °C at $pO_2=10^{-4}$ atm.

1. Introduction

In the solid oxide fuel cell (SOFC) field, the lanthanide nickelates have attracted much attention in the last decade as cathode materials with regards to their mixed ionic-electronic conductivity (MIEC) properties, and more especially to their excellent ionic diffusivity [1–4] and high electronic conductivity at high temperature [5]. For instance, Bassat et al. [2] and Burriel et al. [4] reported that $La_2NiO_{4+\delta}$ exhibits excellent value of the oxygen diffusion coefficient along the *ab* plane, $D^*_{ab} \approx 2\times10^{-8}$ cm^2/s at 600 °C, which is higher than the value obtained for the electrolyte material $Ce_{0.8}Gd_{0.2}O_{2-\delta}$ (GDC) at the same temperature ($D^* \approx 7\times10^{-9}$ cm^2/s). Values at the same temperature are even higher for $Nd_2NiO_{4+\delta}$ ($D^*_{ab} \approx 4\times10^{-8}$ cm^2/s) and $Pr_2NiO_{4+\delta}$ ($D^*_{ab} \approx 8\times10^{-8}$ cm^2/s) [3]. Besides, very low polarization resistances were measured by electrochemical impedance spectroscopy (EIS) for these compounds, as for instance $R_p=80$ mΩ cm^2 at 600 °C for a $Pr_2NiO_{4+\delta}$//$Ce_{0.8}Y_{0.2}O_{2-\delta}$//3mol% Y_2O_3–ZrO_2 half cell [6]. So far, almost all the measurements with the lanthanide nickelates have been carried out in air. However, Kharton et al. [7] and Nakamura et al. [8] studied the behavior of $La_2NiO_{4+\delta}$ down to respectively $pO_2=5\times10^{-4}$ atm and 1×10^{-4} atm, and showed the material to have a very low chemical expansion dependence with oxygen partial pressure. Same observation was reported by Nakamura et al. [9,10] for $Nd_2NiO_{4+\delta}$ down to $pO_2=10^{-4}$ atm. However, no results below 600 °C are available for both materials. For $Pr_2NiO_{4+\delta}$, to our knowledge, no structural studies have been carried out as a function of oxygen partial pressure.

Indeed, it is important to study the behavior of MIEC electrode materials when decreasing pO_2 for at least two reasons. Firstly, under SOFC operation, a MIEC cathode layer may undergo an oxygen non-stoichiometry gradient all along its active volume [7,11], due to the conversion of the electronic current into ionic current as described by Adler et al. [12]. It is then highly desirable for the cathode material to show very little cell volume variation and good chemical stability upon changes of its oxygen non-stoichiometry δ. Secondly, metal supported cell (MSC) using a gas-permeable porous metallic substrate recently

☆DOI: 10.1039/b000000x.
* Corresponding author.
E-mail address: grenier@icmcb-bordeaux.cnrs.fr (J.-C. Grenier).

developed for IT-SOFC application (typically 600–700 °C) are claimed for presenting several advantages in terms of stack design simplicity, low cost fabrication, and better thermal cycling robustness compared to anode or electrolyte supported cells [13–16]. A porous metal is used to support the various layers, the main benefit of this architecture being that the ceramic layers are thin. However, some drawbacks result from this architecture: for instance, it is mandatory not to expose the metal support to oxidizing atmosphere at high temperature during the cell manufacturing. It implies to sinter the constitutive elements of the cell under low pO_2 (*e.g.* under Ar or N_2, $pO_2 \approx 10^{-4}$ atm), or even under H_2. Hence, it is of primary importance for the different layers of the cell to be chemically stable in low oxygen partial pressure atmosphere, and their coefficients of thermal or/and chemical expansion to match in these conditions in order to avoid detrimental delaminations or cracks.

In the scope of the European RAMSES project, lanthanide nickelates $Ln_2NiO_{4+\delta}$ (Ln=La, Pr and Nd) were extensively investigated. Their chemical stability, thermal and chemical expansion when exposed to temperatures as high as 1400 °C, under pO_2 as low as 10^{-4} atm were studied through TGA measurements, *ex situ* and *in situ* XRD analyses, as well as thermal expansion coefficient (TEC) measurements.

2. Experimental

2.1. Lanthanide nickelates preparation

High purity powders were prepared *via* the citrate–nitrate route (modified Pechini method) [17] starting from the precursors Pr_6O_{11} (Aldrich chem, 99.9%), La_2O_3 (Strem Chemical, 99.99%), Nd_2O_3 (Aldrich chem., > 99.9%) and $Ni(NO_3)_2 \cdot 6H_2O$ (Acros Organics, 99%). The lanthanide oxides (Pr_6O_{11}, La_2O_3 and Nd_2O_3) were pre-fired at T=900 °C overnight to remove the water content because of their highly hygroscopic nature. After the combustion step of the nitrate–citrate mixture, a final annealing at 1200 °C for 12 h in air was carried out. Single and well crystallized phases were obtained as confirmed by X-ray diffraction.

2.2. Thermal gravimetry analysis

The thermal behavior and oxygen over-stoichiometry δ of the $Ln_2NiO_{4+\delta}$ (Ln=La, Pr or Nd) materials were studied by thermal gravimetry analysis (TGA) measurements with a Setaram set up (MTB 10-8 balance) under different oxygen partial pressures (pO_2 ranging from 2×10^{-1} down to 10^{-4} atm) and over the temperature range 25–1000 °C at 1 °C/min rate.

2.3. X-ray diffraction analysis

Structural features and phase stability of the lanthanide nickelates were investigated by X-ray powder diffraction using a PANalytical X'Pert Pro X'Celerator diffractometer: *i)* for the *ex situ* measurements performed at room temperature (RT), it was a Cu K_α radiation, *ii)* for the lanthanide nickelates and the electrolyte materials (8YSZ, Tosoh Co., and GDC, Rhodia Comp.), the *in situ* XRD experiments either in air or under helium ($pO_2 \approx 10^{-4}$ atm) were carried out at decreasing temperature with a Co K_α radiation, from 1400 °C down to RT. A heating rate of 2 °C/min was applied to reach the maximum temperature. After two hours of stabilization, two consecutive X-Ray diffractograms were recorded to control that the thermodynamic equilibrium was reached. The time span to record one diffractogram was around 4 h. The sample was then cooled down to a lower temperature, at the cooling rate 2 °C/min. The diffractogram of the sample was recorded after 1 h of stabilization at the defined temperature, *etc.* down to RT. For all the quoted measurements, pO_2 was measured at the outlet of the set up chamber with an Ir/IrO_2 oxygen sensor.

The X-ray diffractograms were fitted by profile matching using the Fullprof software [18]. Typical results are given in Fig. 1.

The values of the thermal expansion coefficients (TEC) were calculated from the thermal variation of the cell volume of the material.

2.4. Dilatometry measurements

The dilatometry measurements were carried out using a differential dilatometer (Netzsch® 402 ED). Sintering curves of 8YSZ, GDC and of the electrode materials ($Ln_2NiO_{4+\delta}$, with Ln=La, Pr or Nd) were measured in air using a green pellet of the corresponding material, at increasing temperature from RT up to 1400 °C, with the heating rate 5 °C/min.

3. Results and discussion

3.1. Chemical stability of the lanthanide nickelates at low pO_2 over the temperature range 25–1300 °C

In a first stage, the chemical stability of the $Ln_2NiO_{4+\delta}$ materials was studied by thermal gravimetry analysis at T < 1000 °C, under various pO_2, combined with post-mortem XRD measurements. The oxygen content of the compounds was determined at RT after the following procedure: the powders were first heated in air up to 1000 °C, then cooled down to RT at 2 °C min^{-1}, this cycle being carried out twice to control its reproducibility. The third cycle consisted in decomposing the materials under Ar – 5% H_2, starting from 1000 °C down to RT at 0.5 °C/min, allowing to determine the RT oxygen content of the lanthanide nickelates as reported in references [19, 20].

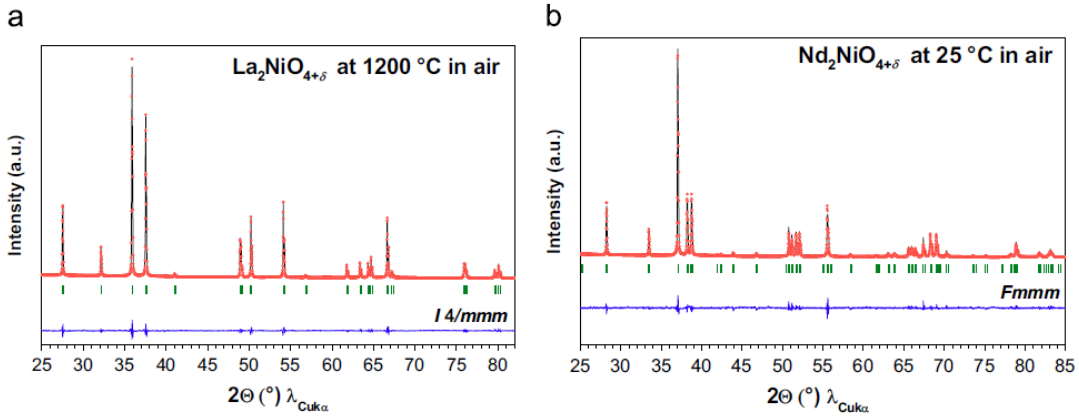

Fig.1. Typical *in situ* X-ray diffractograms in air of: (a) $La_2NiO_{4+\delta}$ at 1200 °C and (b) $Nd_2NiO_{4+\delta}$ at RT. Data have been fitted using the Fullprof software.

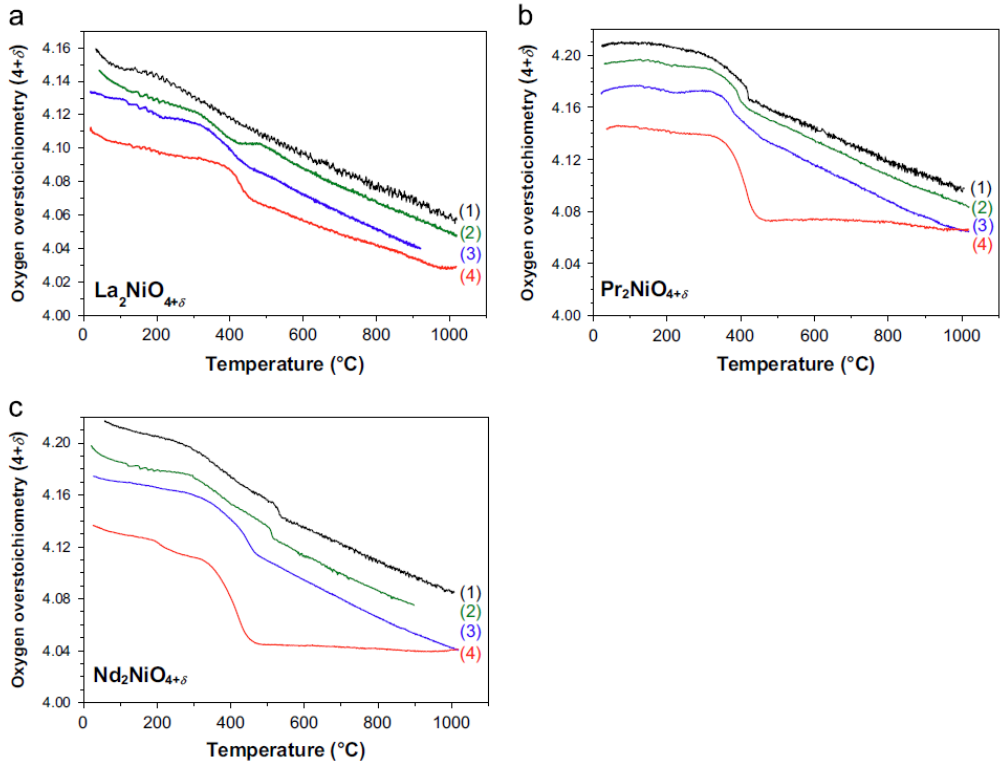

Fig.2. Temperature and pO_2 dependences of the oxygen over-stoichiometry of: (a) $La_2NiO_{4+\delta}$ (b) $Pr_2NiO_{4+\delta}$ and (c) $Nd_2NiO_{4+\delta}$. pO_2=(1) 2×10^{-1} atm, (2) 10^{-2} atm, (3) 10^{-3} atm, (4) 10^{-4} atm.

The temperature and pO_2 dependences of the lanthanide nickelates over-stoichiometry δ are shown in Fig. 2.

Oxygen losses of the lanthanide nickelates are observed at increasing temperature up to 1000 °C, and at decreasing oxygen partial pressure down to 10^{-4} atm. For all the nickelates, the oxygen loss is reversible *vs.* the temperature whatever the oxygen partial pressure is. In addition, XRD characterizations performed after the experiments (not reported here) show that the K_2NiF_4–type structural feature is retained for all the compounds.

The oxygen over-stoichiometry δ decreases approximately of $\Delta\delta\approx0.10$ for $La_2NiO_{4+\delta}$ and $Pr_2NiO_{4+\delta}$, and $\Delta\delta\approx0.14$ for $Nd_2NiO_{4+\delta}$ in between RT and 1000 °C. All nickelates exhibit a variation in their oxygen stoichiometry at about 400–500 °C, which will be discussed in detail in the *in situ* XRD measurements part (Section 3.2).

In a second stage, the chemical stability of the lanthanide nickelates was studied for 1000 °C < *T* < 1300 °C. X-ray diffractograms s were recorded at RT, after heating the materials either in air or nitrogen ($pO_2=10^{-4}$ atm), up to 1300 °C, then cooling down to RT at 3 °C/min. The lattice parameters calculated by profile matching of the XRD data (using the Fullprof program), the space group as well as the thermal stability of the cathode materials are discussed below.

Fig. 3a shows that the lanthanum nickelate phase remains stable after a thermal treatment at 1300 °C, for 2 h either in air or in nitrogen. Some peaks are slightly shifted after the thermal treatment under nitrogen, but a subsequent annealing at 600 °C, in air for 6 h, is sufficient to recover the initial lattice parameters (Table 1). Based on former studies [21], the data obtained in air were refined using the space group *Fmmm* (orthorhombic symmetry). For $La_2NiO_{4+\delta}$ annealed under nitrogen, the refinement was preferentially carried out with the *Bmab* space group, which is of lower symmetry than the *Fmmm* one, due to the occurrence of extra peaks at $2\theta_{Cu}=37.38°$ and $2\theta_{Cu}=39.42°$ ($K\alpha_{1(Cu)}$ radiation).

The praseodymium nickelate remains also stable after a thermal treatment at 1300 °C in air (Fig. 3b). Under low oxygen partial pressure, modifications of the diffraction peaks at $2\theta_{Cu}=33°$, 43° and 44° (see arrows in the figure) take place. Refinement of the XRD data by profile matching was only possible using a mixture of two K_2NiF_4–type phases of orthorhombic symmetry, respectively *Fmmm* and *Bmab*. $Pr_2NiO_{4+\delta}$ stability under low pO_2 will be extensively discussed in the *in situ* XRD measurements part. Nevertheless, after annealing at 600 °C, in air, for 6 h, these peak modifications are totally reversible (Table 1).

The neodymium nickelate also remains stable after a heat treatment at 1300 °C in air, for 2 h (Fig. 3c). The refinement of the data was achieved using the *Fmmm* space group (Table 1). However, under low oxygen partial pressure (*i.e.* $pO_2=10^{-4}$ atm), $Nd_2NiO_{4+\delta}$ was partially decomposed into Nd and Ni oxides above 1000 °C. Unlike $Pr_2NiO_{4+\delta}$, an oxidation step at 600 °C in air was not sufficient to recover the $Nd_2NiO_{4+\delta}$ phase; raising the oxidation temperature up to 950 °C was necessary.

It can be concluded from these measurements that all the nickelates are chemically stable in air up to 1300 °C. Under $pO_2=10^{-4}$ atm, $La_2NiO_{4+\delta}$ and $Pr_2NiO_{4+\delta}$ retains their structure, while $Nd_2NiO_{4+\delta}$ is partially decomposed into Nd_2O_3 and NiO above 1000 °C. Knowing the temperature range where the materials are chemically stable, the next step of this study was to record *in situ* X-ray diffractograms of the materials either in air or under low $pO_2=10^{-4}$ atm.

3.2. High temperature in situ XRD measurements at low pO_2

3.2.1. $La_2NiO_{4+\delta}$

X-ray diffractograms of $La_2NiO_{4+\delta}$ are shown in Fig. 4 and the results of refinements in Fig. 5. The structure of the

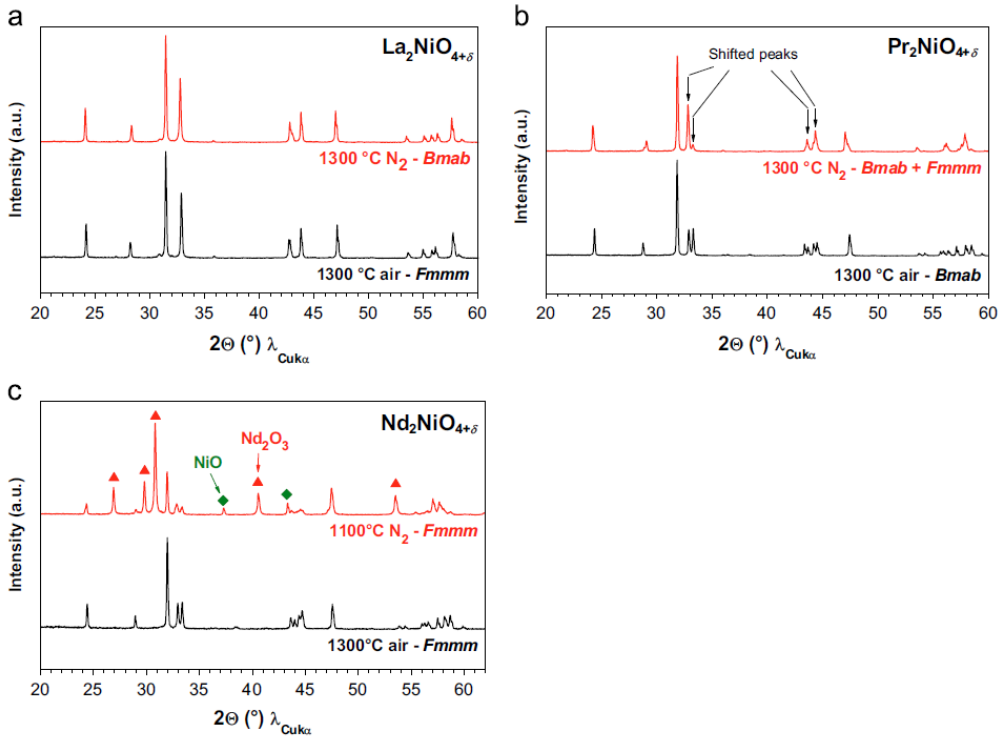

Fig.3. X-ray diffractograms of (a) $La_2NiO_{4+\delta}$, (b) $Pr_2NiO_{4+\delta}$ and (c) $Nd_2NiO_{4+\delta}$ after heat treatment in air or nitrogen ($pO_2 = 10^{-4}$ atm) atmosphere at 1300 °C or 1100 °C.

Table 1
Starting shrinkage temperature and maximum shrinkage rate temperature of the electrode and electrolyte materials in air.

Compound	Sintering atm.	Lattice parameters (Å)			Space group
		a	*b*	*c*	
$La_2NiO_{4+\delta}$	Air	5.4585	5.4658	12.6867	*Fmmm*
	N_2	5.4722	5.4772	12.6259	*Bmab*
	N_2 + reox.	5.4597	5.4647	12.6802	*Fmmm*
$Pr_2NiO_{4+\delta}$	Air	5.3934	5.4565	12.4461	*Bmab*
	N_2	–	–	–	–
	N_2 + reox.	5.4571	5.3946	12.4462	*Bmab*
$Nd_2NiO_{4+\delta}$	Air	5.3796	5.4435	12.3594	*Fmmm*
	N_2	–	–	–	–
	N_2 + reox.	5.3773	5.4456	12.3597	*Fmmm*

over-stoichiometric $La_2NiO_{4+\delta}$ compound annealed in air, with $\delta > 0.13$, has been previously determined by Jorgensen et al. [22] and Skinner [21] using neutron diffraction data to be *Fmmm*-type below 150 °C. It consists of non-tilted NiO_6 octahedra whose strains have been released due to the partial oxidation of Ni^{2+} into Ni^{3+} [23]. At $T > 150$ °C, the symmetry of the $La_2NiO_{4+\delta}$ cell changes from orthorhombic (*Fmmm* SG) to tetragonal (*I4/mmm* SG) [21,24]. Indeed, at high temperature the thermal agitation is high enough to stabilize the structure in a higher symmetry, in which the apical oxygen of the NiO_6 octahedra is no more split into two positions.

In our material, the δ value is larger than 0.14 for $T < 150$ °C, as shown by the TGA data in Fig. 2a. Hence, the *Fmmm* and then *I4/mmm* space groups were used to fit our data, in agreement with [19].

Fig. 5a shows that the values of the *a*, *b* and *c* lattice parameters linearly increase with temperature, which can be attributed to the thermal expansion of the material, as proposed by Skinner [21]. At around 150 °C, the change of symmetry from *Fmmm* to *I4/mmm* results in the conjunction of the *a* and *b* lattice parameter values. Absolute values obtained for the lattice parameters are comparable to the ones obtained by Aguadero et al. [25] for $La_2NiO_{4.30}$, from RT up to 700 °C. In Fig. 5b, the evolution of the *c* lattice parameter has been plotted together with the over-stoichiometry δ *vs.* the temperature. A slight change in the slope of the *c* parameter occurs at around 300 °C, which however could not be related with the symmetry change.

As shown by previous authors [23,26], in order to avoid distortions in the K_2NiF_4–type structure of $La_2NiO_{4+\delta}$, interstitial oxygen can be accommodated inside the La_2O_2 rocksalt-type layers (Fig. 6). Insertion of O_2 in the structure leads to an increase of the *c* lattice parameter, while the subsequent oxidation of Ni^{2+} into Ni^{3+} leads to a decrease of the *a* and/or *b* lattice parameters [7,23,27]. Hence, the *c* lattice parameter should be decreasing in parallel with the over-stoichiometry δ. However, the results show that the *c* lattice parameter linearly increases with temperature, while the oxygen over-stoichiometry decreases almost linearly. Actually, the expected decrease of the *c* lattice parameter is canceled by the lattice thermal expansion, which is by far higher.

Under He ($pO_2 = 10^{-4}$ atm), Fig. 4b points out a different behavior of the material at $T < 450$ °C compared to air. Indeed, the (110) peak at $2\theta_{Co} \approx 38°$ splits into two other distinct ones. In addition, the presence of diffraction peaks at $2\theta_{Co} = 43.37°$ and $2\theta_{Co} = 46.13°$ ($K\alpha_{1(Co)}$ radiation, not reported) could be observed, which leads to propose that under low pO_2 and $T < 450$ °C, $La_2NiO_{4+\delta}$ no longer adopts the *Fmmm* space group, but rather the *Bmab* one. Then for $T > 450$ °C, Fig. 4b shows that the (020) and (200) peaks merge into one, which characterizes the change in space group from orthorhombic *Bmab* to tetragonal *I4/mmm*.

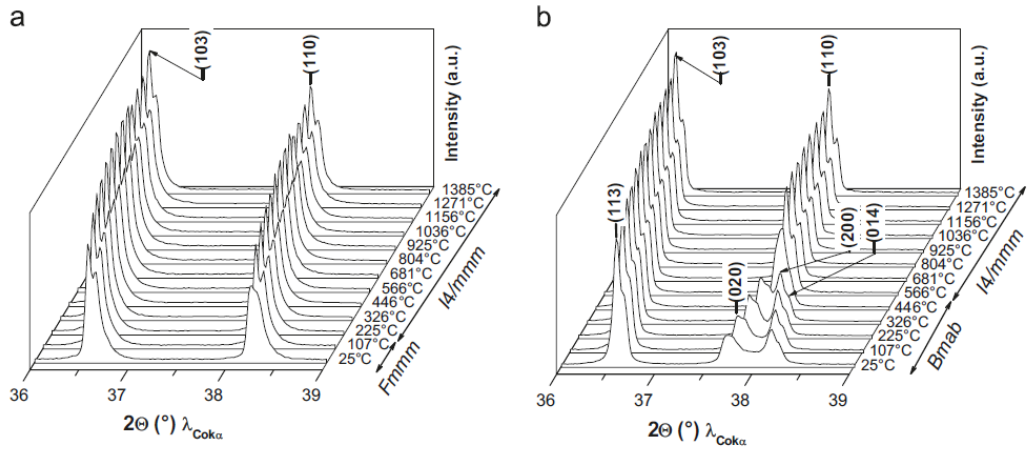

Fig. 4. Thermal evolution of the X-ray diffractograms of $La_2NiO_{4+\delta}$ (a) in air and (b) under He ($pO_2 = 10^{-4}$ atm).

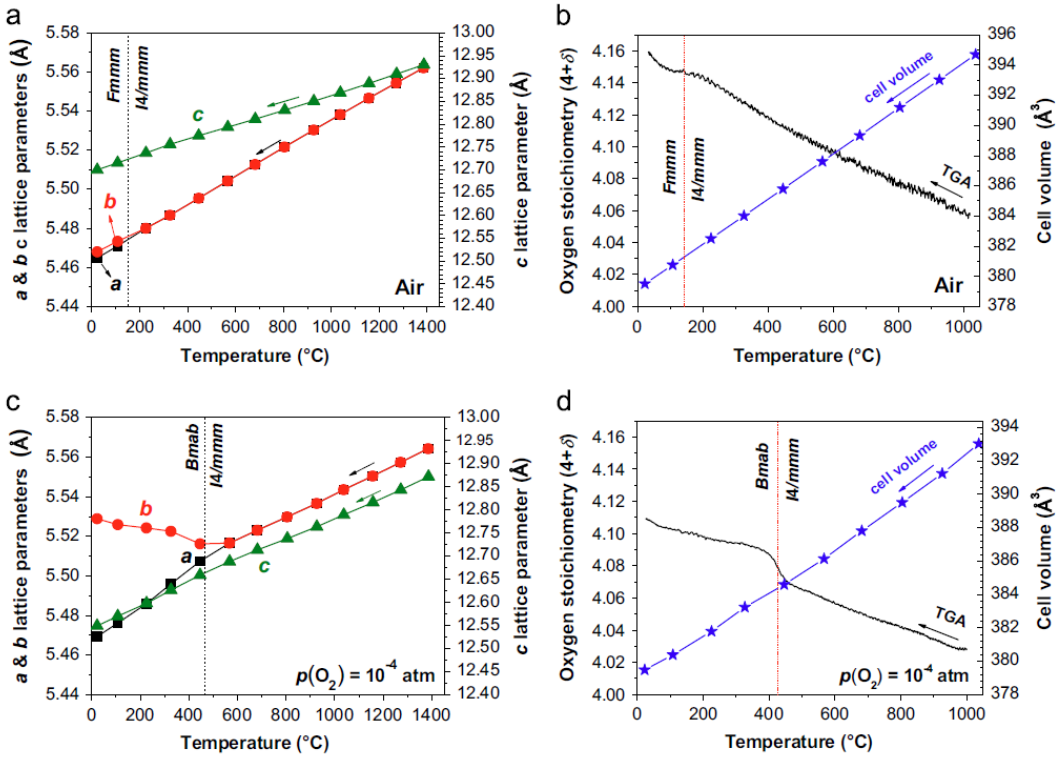

Fig. 5. Thermal variation of the lattice parameters of $La_2NiO_{4+\delta}$ under air (a) and $pO_2 = 10^{-4}$ atm (c). Thermal variation of the cell volume and of the oxygen over-stoichiometry δ of $La_2NiO_{4+\delta}$ under air (b) and $pO_2 = 10^{-4}$ atm (d).

This transition is also clearly visible in the TGA plot (Fig. 5d), together with the change of the slope of *a*, *b* and *c* lattice parameter variations (Fig. 5c).

The relative variations of the lattice parameter values α_i and of the cell volume α_v when the oxygen partial pressure is decreased from 0.2 atm (air) to 10^{-4} atm (He) have been reported in Fig. 7, using Eqs. (1) and (2), respectively:

$$\alpha_i = \frac{\text{lattice parameter } i \text{ value}_{(\text{helium})} - \text{lattice parameter } i \text{ value}_{(\text{air})}}{\text{lattice parameter } i \text{ value}_{(\text{air})}} \times 100 \quad (1)$$

$$\alpha_v = \frac{\text{cell volume}_{(\text{helium})} - \text{cell volume}_{(\text{air})}}{\text{cell volume}_{(\text{air})}} \times 100 \quad (2)$$

Results indicate that, in the whole temperature range 25–1200 °C, the *c* lattice parameter value is always lower in helium than in air. This can be directly related to the lower value of the over-stoichiometry δ of $La_2NiO_{4+\delta}$ in low pO_2 (*cf.* Fig. 2a). For $T < 450$ °C, the decrease in the value of the *c* lattice parameter is preferentially counterbalanced by an increase of the *b* lattice parameter, the *a* lattice parameter keeping the same value than in air. This implies that the shortening of the metal-oxygen bond between Ni and the apical oxygen at low pO_2 is compensated by an increase of the Ni–O bond between Ni and the equatorial oxygen, but mostly along the *b* direction.

3.2.2. $Pr_2NiO_{4+\delta}$

In air, $Pr_2NiO_{4+\delta}$ undergoes a structural change from *Bmab* to *I4/mmm* at around 400 °C (Fig. 8a), in agreement with previous results of Allançon et al. [28,29].

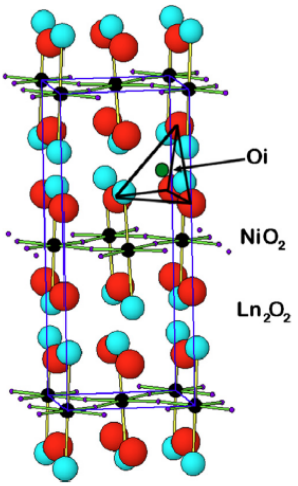

Fig.6. Orthorhombic structure of $Ln_2NiO_{4+\delta}$ phases. showing as an example the oxygen interstitial in La tetrahedron of the La_2O_2 layer.

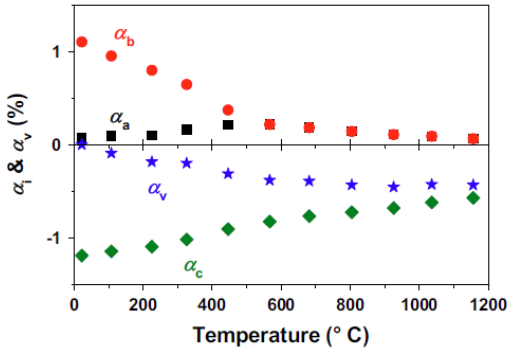

Fig. 7. Thermal relative variation of the lattice parameters and of the cell volume of $La_2NiO_{4+\delta}$ when pO_2 is decreased from 0.2 atm (air) to 10^{-4} atm (He). (■) α_a (●) α_b (◆) α_c (★) α_v.

As mentioned for $La_2NiO_{4+\delta}$, the lattice parameters increase with the temperature due to the thermal expansion. The slope of this increase differs depending on $Pr_2NiO_{4+\delta}$ space group (Fig. 9a).

Under low pO_2, and to the author's knowledge, the structure (*i.e.* the symmetry) of the over-stoichiometric $Pr_2NiO_{4+\delta}$ cell has not been yet resolved. In this study, the material undergoes a structural transition at around 400 °C, as observed in air. During this transition, the lattice parameter *c* value largely drops, which can be directly correlated with the loss of interstitial oxygen observed by TGA (*cf.* Fig. 2d).

In Fig. 8b and Fig. 9c, it is noteworthy that the *a* and *b* lattice parameters are never equal over the whole temperature range, which means that the tetragonal symmetry is not reached for $Pr_2NiO_{4+\delta}$ under low pO_2. The X-ray diffractograms were accurately fitted using the *Bmab* space group, the *Fmmm* one being ruled out due to presence of extra peaks; in-depth studies would however be needed in order to confirm the relevance of the chosen space group.

In Fig. 10, no significant variation of the lattice parameters of $Pr_2NiO_{4+\delta}$ is observed in the temperature range 25 °C < *T* < 350 °C when pO_2 is decreased from air down to $pO_2 = 10^{-4}$ atm. It indicates that the $Pr_2NiO_{4+\delta}$ lattice parameters values are more or less the same at low pO_2 than in air in this temperature range. However for *T* > 400 °C, the behavior is somewhat different since the material undergoes a symmetry change from tetragonal to orthorhombic when pO_2 is decreased. The *b* lattice parameter keeps the same value as in air, whereas the *c* parameter decreases and *a* increases in compensation. One should stress that both features make the cell volume to remain almost constant as pO_2 decreases, which is particularly interesting for cathode materials (see below).

3.2.3. $Nd_2NiO_{4+\delta}$

For $Nd_2NiO_{4+\delta}$, the *in-situ* X-ray diffractograms recorded in air (Fig. 11a) show that the symmetry of the cell changes at around 500 °C. Based on literature data [30–32] for $Nd_2NiO_{4+\delta}$ with $0.13 \leq \delta \leq 0.25$, the low and high temperature structures have been respectively refined using *Fmmm* and *I4/mmm* space groups. Indeed, the values of the lattice parameters at room temperature, *i.e.* *a* = 5.375 Å, *b* = 5.455 Å and *c* = 12.36 Å for $\delta = 0.22$, are very close to those reported by Ishikawa et al. [32] for $\delta = 0.223$, which were refined using the *Fmmm* orthorhombic symmetry. Apart from the structural transition at around 400 °C, the increase of the lattice parameters with the temperature (Fig. 12a) is mainly due to thermal expansion as observed for $La_2NiO_{4+\delta}$ and $Pr_2NiO_{4+\delta}$.

To the author's knowledge, no structural characterization of $Nd_2NiO_{4+\delta}$ at low pO_2 has been previously reported in the

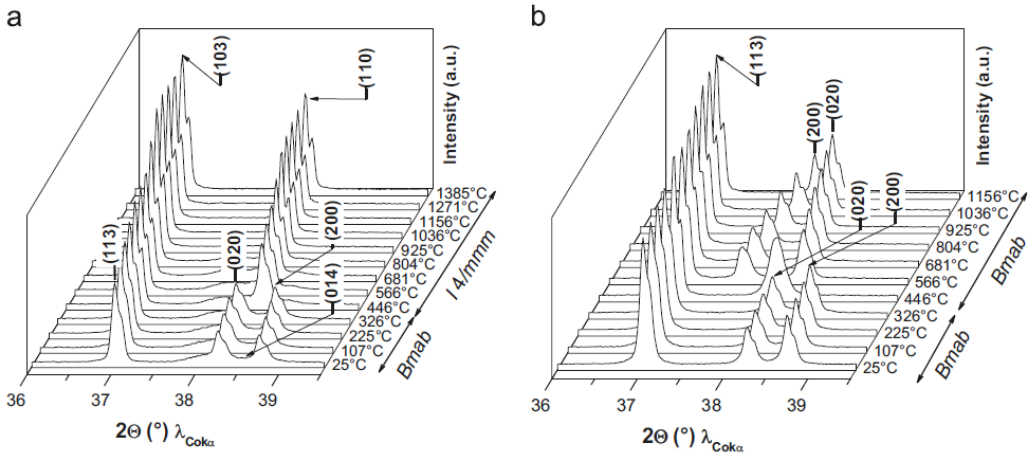

Fig. 8. Thermal evolution of the X-ray diffractograms of $Pr_2NiO_{4+\delta}$: (a) in air and (b) under He ($pO_2 = 10^{-4}$ atm).

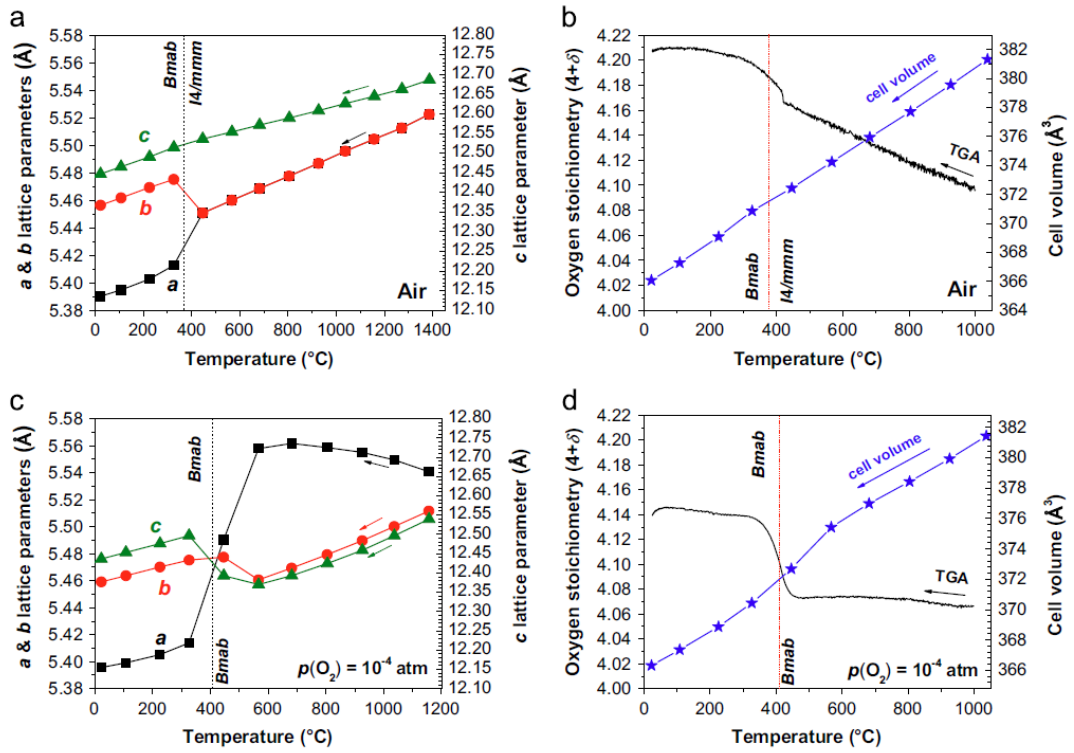

Fig.9. Thermal variation of the lattice parameters of $Pr_2NiO_{4+\delta}$ under air (a) and $pO_2=10^{-4}$ atm (c). Thermal variation of the cell volume and of the oxygen over-stoichiometry δ of $Pr_2NiO_{4+\delta}$ under air (b) and $pO_2=10^{-4}$ atm (d).

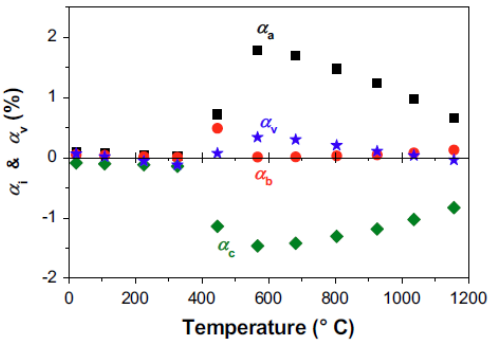

Fig. 10. Thermal relative variation of the lattice parameters and of the cell volume of $Pr_2NiO_{4+\delta}$ when pO_2 is decreased from 0.2 atm (air) down to 10^{-4} atm (He). (■) α_a (●) α_b (♦) α_c (★) α_v.

literature. In this study (Fig. 11b), the X-ray diffractograms clearly show that the structure of the nickelate remains orthorhombic over the whole temperature range at low pO_2. The best fit of the data was obtained using the *Fmmm* space group, but further studies would be needed to confirm this point. Interestingly, the transition at around 400 °C (Fig. 12d) evidenced by the large drop in δ in the TGA curves is not concomitant with a drop of the *c* cell constant, as previously observed for $Pr_2NiO_{4+\delta}$ at low pO_2 (Fig. 9d). Actually, the transition goes together with a peculiar variation of *a* and *b* lattice parameters at high temperature (Fig. 12c), which mainly differs from a linear thermal expansion as observed in air (Fig. 12a).

In Fig. 13, it is noteworthy that, when pO_2 drops from 0.2 atm (air) down to 10^{-4} atm (He), the decrease of the *c* parameter is counter-balanced over the whole temperature range by an increase of the *a* lattice parameter as observed for $Pr_2NiO_{4+\delta}$ for $T > 400$ °C (*cf.* Fig. 10); the *b* lattice parameter keeps almost the same value than in air.

Finally, comparison of Figs. 7, 10 and 13, which report the chemical expansion of the cell volume of respectively $La_2NiO_{4+\delta}$, $Pr_2NiO_{4+\delta}$ and $Nd_2NiO_{4+\delta}$, shows that whatever the lanthanide nickelate, the chemical expansion of the material between 25 °C and 1200 °C (at least) is below 0.5%, which is very low compared to other commercial electrode materials for SOFC such as LSC [10,33].

During SOFC operation, it is known [7] that thermal cycling induces changes in the oxygen stoichiometry of the MIEC material. In addition, high current densities also cause oxygen non-stoichiometry gradients in the electrode resulting in chemical stresses [11].

However, since the lanthanide nickelates exhibit very low chemical expansion as a function of pO_2, it is expected for these materials to be highly robust as cathode active layers in a SOFC electrode architecture.

3.3. *Determination of the shrinkage and of the TEC in air and under low pO_2*

Another issue concerning the fuel cell robustness is the matching between the thermal expansion coefficients (TECs) of the different layers, as for instance the electrode layer, the interfacial layer and the electrolyte support for a $Ln_2NiO_{4+\delta}$//GDC//YSZ half-cell. Indeed, when manufacturing a SOFC cell, it is mandatory to know the shrinkage behavior of the different layers, as well as to determine the temperature at which necks between the electrode grains will appear, in order to yield efficient electronic/ionic conduction. Furthermore, these data are useful when managing a co-sintering process of different layers during cell manufacturing.

Shrinkages of the electrode and electrolyte materials were deduced from dilatometry measurements in air. Results are reported in Fig. 14; in addition, the temperature at which the

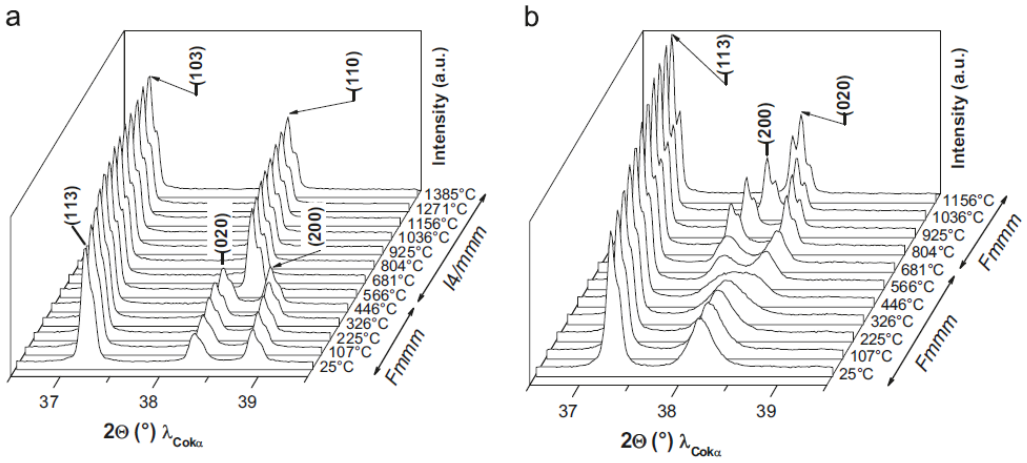

Fig. 11. Thermal evolution of the X-ray diffractograms of $Nd_2NiO_{4+\delta}$: (a) in air or (b) under He ($pO_2=10^{-4}$ atm).

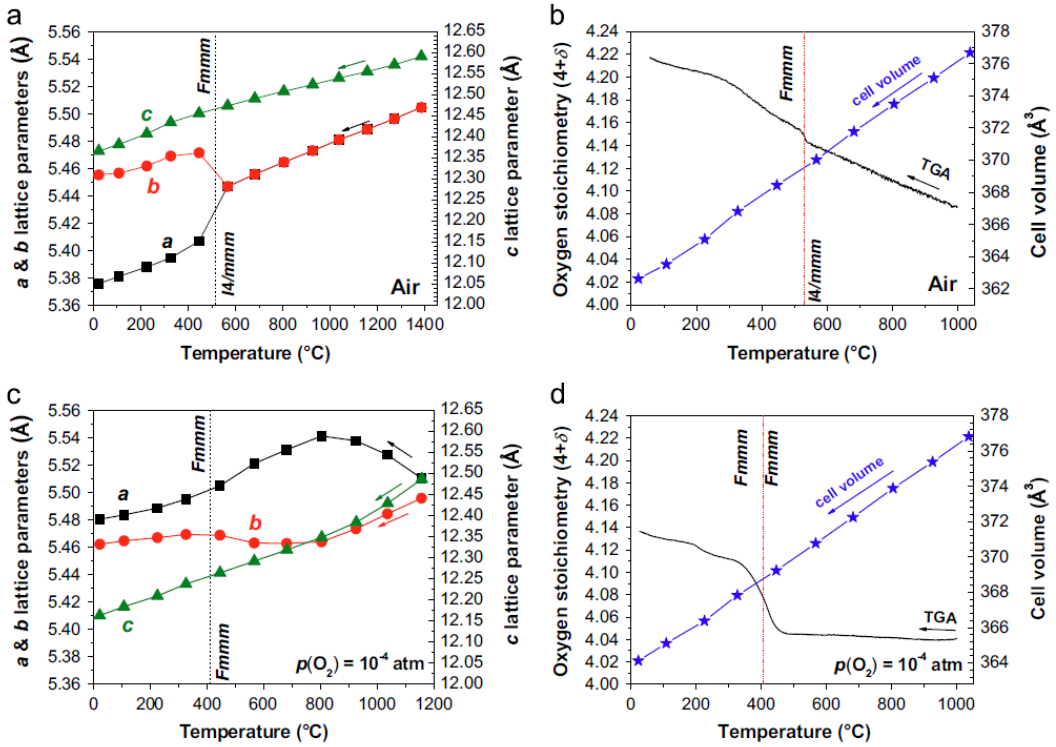

Fig. 12. Thermal variation of the lattice parameters of $Nd_2NiO_{4+\delta}$ under air (a) and $pO_2=10^{-4}$ atm (c). Thermal variation of the cell volume and of the oxygen over-stoichiometry δ of $Nd_2NiO_{4+\delta}$ under air (b) and $pO_2=10^{-4}$ atm (d).

sintering of the material starts, along with the temperature at which the shrinkage rate is the highest are given in Table 2.

Firstly, results show that the shrinkage of the GDC interfacial layer begins at $T\approx 650$ °C, $Pr_2NiO_{4+\delta}$ at $T\approx 900$ °C, and finally 8YSZ, $La_2NiO_{4+\delta}$ and $Nd_2NiO_{4+\delta}$ at around 1100 °C. These results are important for SOFC application as they indicate that higher temperatures of annealing should be used in order to obtain well sintered porous electrode layers.

Secondly, it is noteworthy that the highest rate of sintering happens at $T\approx 840$ °C for GDC, $T\approx 1140$ °C for $Pr_2NiO_{4+\delta}$, and $T\approx 1330$ °C for 8YSZ, $La_2NiO_{4+\delta}$ and $Nd_2NiO_{4+\delta}$. For all the compounds, except $Pr_2NiO_{4+\delta}$, the shrinkage of the pellets is not complete at 1400 °C.

The thermal expansion coefficients (TECs) were calculated from *in situ* XRD data acquisition either in air or under helium ($pO_2=10^{-4}$ atm), for the 8YSZ electrolyte and the GDC interfacial layer with the aim to be compared with those of the lanthanide nickelates also calculated from the *in situ* high temperature XRD data. The variation of the cell volume of 8YSZ and GDC is reported in Fig. 15.

Both 8YSZ and GDC were fitted using the cubic *Fm-3m* space group, either in air or under $pO_2=10^{-4}$ atm, from RT up to around 1300 °C. If the variation of the cell volume was linear *vs.* the

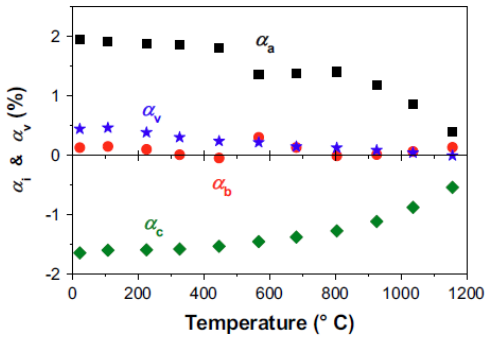

Fig. 13. Relative thermal variation of the lattice parameters α_i and of the cell volume α_v for $Nd_2NiO_{4+\delta}$ when pO_2 is decreased from 0.2 atm (air) down to 10^{-4} atm (He). (■) α_a (●) α_b (♦) α_c (★) α_v.

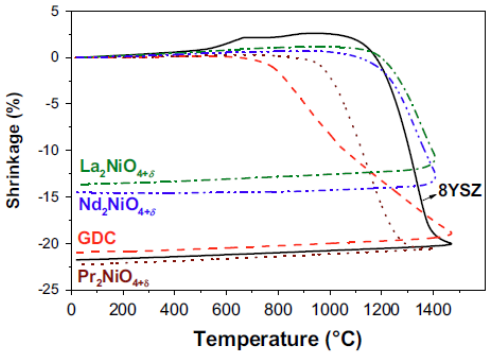

Fig. 14. Shrinkage curves of the electrode and electrolyte materials in air. Heating rate: 5 °C/min.

temperature for both material in air, variation of the slope were observed under He. This behavior is discussed below in terms of TEC.

The variation of the thermal expansion coefficients of the electrode and electrolyte material either in air or at low pO_2 *vs.* temperature is reported in Fig. 16.

In air, the TECs of the electrolyte and of the electrode materials are quite close from each other on the whole temperature range. In agreement with previous results from the literature [20,34,35] the TEC of the GDC interlayer ($\approx 12.2\times10^{-6}\,K^{-1}$) is in between the TEC of the 8YSZ electrolyte ($\approx 10.4\times10^{-6}\,K^{-1}$) and the TECs of the lanthanide nickelates ($>11.1\times10^{-6}\,K^{-1}$). Besides its role as barrier layer to cations diffusion, it should be expected from the GDC interlayer to act as a buffer between the low thermal expansion coefficient of the electrolyte, and the highest one's of the electrodes. At $T<400$ °C, the TEC of $Pr_2NiO_{4+\delta}$ slightly increases from $13.4\times10^{-6}\,K^{-1}$.up to $14.2\times10^{-6}\,K^{-1}$, which is still quite acceptable. The TEC of $Nd_2NiO_{4+\delta}$ decreases from $12.4\times10^{-6}\,K^{-1}$ down to $11.1\times10^{-6}\,K^{-1}$, which is in between the TEC values of 8YSZ and GDC. For all the electrodes, these variations are related to changes in the crystal symmetry of the materials from orthorhombic to tetragonal at around 400 °C, except for $La_2NiO_{4+\delta}$ that keeps the same TEC$=13.0\times10^{-6}\,K^{-1}$ over the whole temperature range.

To conclude for the experiments performed in air, a temperature of at least 900 °C should be reached to initiate the shrinkage of $Pr_2NiO_{4+\delta}$, and at least 1100 °C for $La_2NiO_{4+\delta}$ or $Nd_2NiO_{4+\delta}$ (Table 2) In this temperature range, the TEC matching between the electrolyte and the electrode materials are quite good (Fig. 16a).

At low pO_2, again the X-ray diffractograms of 8YSZ and GDC were both accurately fitted using the cubic *Fm-3m* space group, from RT up to 1200 °C. As expected, the variation of the cell volume of 8YSZ does not depend on pO_2, However, a slight variation of its

Table 2
Lattice parameters of $Ln_2NiO_{4+\delta}$ phases (profile matching of XRD data). Standard deviations for: a and $b<0.0002$, $c<0.0004$.

Compounds	Sintering plot	
	Starting T (°C)	Max. shrinkage rate T (°C)
8YSZ	1080	1330
GDC	650	840
$La_2NiO_{4+\delta}$	1100	1350
$Pr_2NiO_{4+\delta}$	900	1140
$Nd_2NiO_{4+\delta}$	1070	1330

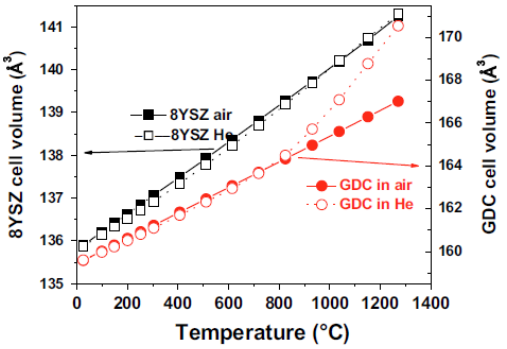

Fig. 15. Thermal variation of the cell volume of the electrolyte materials, 8YSZ and GDC, in air or under He ($pO_2=10^{-1}$ atm).

TEC from $9.1\times10^{-6}\,K^{-1}$ up to $11.3\times10^{-6}\,K^{-1}$ appears at around 450 °C. Unlike, GDC exhibits an increase of the cell volume in He with regard to air, above 800 °C, which results in a large increase of the TEC from $11.9\times10^{-6}\,K^{-1}$ up to $29.8\times10^{-6}\,K^{-1}$: it is likely to be due to a loss of oxygen of GDC in these low pO_2 conditions, associated with the reduction of Ce^{4+} into Ce^{3+}.

Apart from GDC, the same match than in air was observed between the TECs of 8YSZ and of the electrode materials, from RT up to 1200 °C (Fig. 16b). For $T<500$ °C, variations of the TECs for both the electrodes and 8YSZ materials were observed, but the matching between the layers was still good, the TECs ranging between 9.1 and 12.2. The matching with GDC is very good up to around 800 °C; however beyond this temperature, the TEC of GDC largely increases (TEC$=29.8\times10^{-6}\,K^{-1}$): thermal cycling at $T>800$ °C should then be avoided under atmosphere poor in oxygen.

4. Conclusion

This study aimed to provide useful data concerning the structural features of the lanthanide nickelates $Ln_2NiO_{4+\delta}$ (Ln=La, Pr or Nd) for temperatures ranging from RT up to a maximum of 1400 °C, either in air or in neutral gas with low $pO_2=10^{-4}$ atm. In addition, the shrinkage behavior of these lanthanide nickelates was studied, and their thermal expansion coefficients (TECs) as well as those of the SOFC electrolyte materials such as 8YSZ and GDC were measured. $La_2NiO_{4+\delta}$ proved to be chemically very stable, even at high temperature and low pO_2, and remained oxygen over-stoichiometric whatever the studied temperature and pO_2. It always keeps the K_2NiF_4-type structure, the symmetry changing from orthorhombic to tetragonal at around 150 °C in air or 400 °C at $pO_2=10^{-4}$ atm. A similar behavior was observed for $Pr_2NiO_{4+\delta}$ and $Nd_2NiO_{4+\delta}$, the only differences being that their respective symmetry remains orthorhombic at $pO_2=10^{-4}$ atm over the whole temperature range; the structural transition occurring at around 400 °C, either in air or at low pO_2, seems

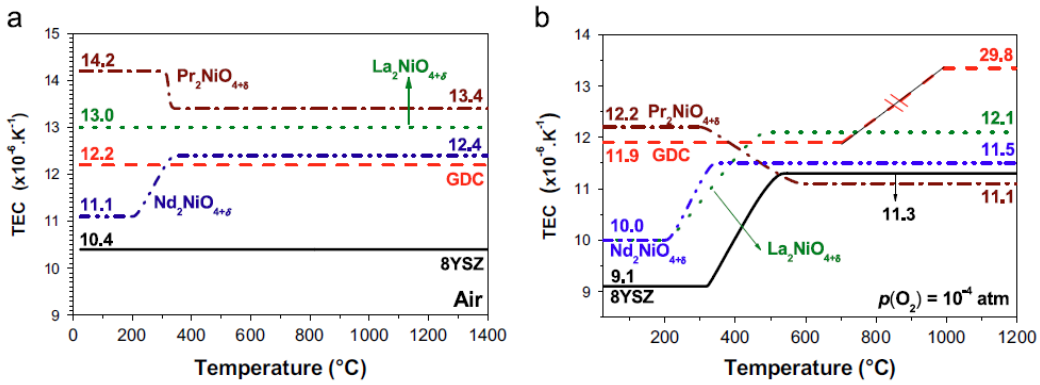

Fig. 16. Thermal expansion coefficients of the electrode and electrolyte materials (a) in air or (b) at low $pO_2 = 10^{-4}$ atm *vs.* the temperature, calculated by *in situ* XRD measurements.

not to induce a change of space group. In addition, $Nd_2NiO_{4+\delta}$ decomposes into Nd_2O_3 and NiO above 1000 °C under low pO_2, contrarily to $La_2NiO_{4+\delta}$ and $Pr_2NiO_{4+\delta}$ which are chemically stable. Finally, it is worth noting that the cell volume of all these lanthanide nickelates remains unchanged upon decreasing the oxygen partial pressure from 0.2 atm down to 10^{-4} atm, at a given temperature over the range 25–1200 °C, which indicates that the chemical expansion of these compounds is almost nil *vs.* the δ variation. In the scope of using these lanthanide nickelates as cathode materials for fuel cell development, dilatometry measurements revealed that a sintering temperature of at least 900 °C for $Pr_2NiO_{4+\delta}$ and 1100 °C for $La_2NiO_{4+\delta}$ or $Nd_2NiO_{4+\delta}$ has to be reached in order to begin the sintering in air of the raw powder particles, which is of major importance for the resulting electrodes to exhibit good electronic/ionic conduction.

Finally, TECs measurements of these materials compared to the ones of the electrolytes, 8YSZ and GDC, showed that no significant stresses should occur between layers of a $Ln_2NiO_{4+\delta}$//GDC//8YSZ half cell in the temperature range 25 °C ≤ T ≤ 1400 °C, in air. At $pO_2 = 10^{-4}$ atm, the TEC of the lanthanide nickelates and 8YSZ are close from each other in the temperature range 25 °C ≤ T ≤ 1200 °C. The problem comes from GDC: below 800 °C, the TEC of GDC match well those of the lanthanide nickelates and 8YSZ. But beyond 800 °C, the TEC of GDC largely increase up to 29.8×10^{-6} K^{-1}, which is likely to be due to the reduction of Ce^{4+} into Ce^{3+}. Mechanical stresses, with the potential risk of delamination, can be expected for $Ln_2NiO_{4+\delta}$//GDC//8YSZ half cell in these conditions.

References

[1] A. Chroneos, D. Parfitt, J.A. Kilner, R.W. Grimes, J. Mater. Chem. 20 (2010) 266–270.
[2] J.M. Bassat, P. Odier, A. Villesuzanne, C. Marin, M. Pouchard, Solid State Ion. 167 (2004) 341–347.
[3] J.-M. Bassat, M. Burriel, O. Wahyudi, R. Castaing, M. Ceretti, P. Veber, I. Weill, A. Villesuzanne, J.-C. Grenier, W. Paulus, J.A. Kilner, J. Phys. Chem. C 117 (2013) 26466–26472.
[4] M. Burriel, J. Santiso, M.D. Rossell, G. Van Tendeloo, A. Figueras, G. Garcia, J. Phys. Chem. C 112 (2008) 10982–10987.
[5] E. Boehm, J.M. Bassat, P. Dordor, F. Mauvy, J.C. Grenier, P. Stevens, Solid State Ion. 176 (2005) 2717–2725.
[6] C. Ferchaud, J.C. Grenier, Y. Zhang-Steenwinkel, M.M.A. van Tuel, F.P.F. van Berkel, J.M. Bassat, J. Power Sources 196 (2011) 1872–1879.
[7] V.V. Kharton, A.V. Kovalevsky, M. Avdeev, E.V. Tsipis, M.V. Patrakeev, A.A. Yaremchenko, E.N. Naumovich, J.R. Frade, Chem. Mater. 19 (2007) 2027–2033.
[8] T. Nakamura, Y. Takeyama, S. Watanabe, K. Yashiro, K. Sato, T. Hashida, J. Mizusaki, ECS Trans. 25 (2009) 2573–2580.
[9] T. Nakamura, K. Yashiro, K. Sato, J. Mizusaki, J. Solid State Chem. 182 (2009) 1533–1537.
[10] T. Nakamura, K. Yashiro, K. Sato, J. Mizusaki, Solid State Ion. 181 (2010) 402–411.
[11] A. Bieberle, L.J. Gauckler, Oxygen Ion and Mixed Conductors and Their Technological Applications, Kluwer Academic, Dordrecht, The Netherlands, 2000.
[12] S.B. Adler, Chem. Rev. 104 (2004) 4791–4843.
[13] L. Rose, O. Kesler, C. Decès-Petit, T. Troczynski, R. Maric, Int. J. Green Energy 6 (2009) 638–645.
[14] W.N. Liu, X. Sun, M.A. Khaleel, Fuel Cells 10 (2010) 703–717.
[15] P. Lamp, J. Tachtler, O. Finkenwirth, S. Mukerjee, S. Shaffer, Fuel Cells 3 (2003) 146–152.
[16] N. Christiansen, H. Holm-Larsen, S. Primdahl, M. Wandel, S. Ramousse, A. Hagen, Solid Oxide Fuel Cells, in: S.C. Singhal, K. Eguchi (Eds.), Electrochemical Society Inc, Pennington, 2011, pp. 71–80 12.
[17] P. Courty, H. Ajot, C. Marcilly, B. Delmon, Powder Technol. 7 (1973) 21–38.
[18] T. Roisnel, J. Rodriguez-Carvajal in, in: R. Delhez, E.J. Mittemeijer (Eds.), Epdic 7: European Powder Diffraction, Pts 1 and 2, 378-3, 2001, pp. 118–123.
[19] J.A. Kilner, C.K.M. Shaw, Solid State Ion. 154–155 (2002) 523–527.
[20] E. Boehm, J.M. Bassat, M.C. Steil, P. Dordor, F. Mauvy, J.C. Grenier, Solid State Sci. 5 (2003) 973–981.
[21] S.J. Skinner, Solid State Sci. 5 (2003) 419–426.
[22] J.D. Jorgensen, B. Dabrowski, S. Pei, D.R. Richards, D.G. Hinks, Phys. Rev. B 40 (1989) 2187–2199.
[23] C. Frayret, A. Villesuzanne, M. Pouchard, Chem. Mater. 17 (2005) 6538–6544.
[24] M.T. Fernández-Díaz, J.L. Martínez, J. Rodríguez-Carvajal, Solid State Ion. 63–65 (1993) 902–906.
[25] A. Aguadero, J.A. Alonso, M.J. Martinez-Lope, M.T. Fernandez-Diaz, M.J. Escudero, L. Daza, J. Mater. Chem. 16 (2006) 3402–3408.
[26] L. Minervini, R.W. Grimes, J.A. Kilner, K.E. Sickafus, J. Mater. Chem. 10 (2000) 2349–2354.
[27] V.V. Kharton, A.P. Viskup, A.V. Kovalevsky, E.N. Naumovich, F.M.B. Marques, Solid State Ion. 143 (2001) 337–353.
[28] C. Allançon, A. Gonthier-Vassal, J.M. Bassat, J.P. Loup, P. Odier, Solid State Ion. 74 (1994) 239–248.
[29] C. Allancon, J. Rodriguez-Carvajal, M.T. Fernandez-Diaz, P. Odier, J.M. Bassat, J.P. Loup, J.L. Martinez, Z. Fur Phys. B-Condensed Matter 100 (1996) 85–90.
[30] Y. Takeda, M. Nishijima, N. Imanishi, R. Kanno, O. Yamamoto, J. Solid State Chem. 96 (1992) 72–83.
[31] M. Zaghrioui, F. Giovannelli, N. Poirot, D. Brouri, I. Laffez, J. Solid State Chem. 177 (2004) 3351–3358.
[32] K. Ishikawa, K. Metoki, H. Miyamoto, J. Solid State Chem. 182 (2009) 2096–2103.
[33] X.Y. Chen, J.S. Yu, S.B. Adler, Chem. Mater. 17 (2005) 4537–4546.
[34] H. Hayashi, M. Kanoh, C.J. Quan, H. Inaba, S. Wang, M. Dokiya, H. Tagawa, Solid State Ion. 132 (2000) 227–233.
[35] K. Kordesch, G. Simader, Fuell Cells and Their Applications, Weinheim, Cambridge, 1996.